1   *Revision_1*

2   *Letter to the Editor*

Minerals in cement chemistry: a single-crystal neutron diffraction study of ettringite, Ca6Al2(SO4)3(OH)12·27H2O

G. Diego Gatta[1,2], Ulf Hålenius [3], Ferdinando Bosi[4],

Laura Cañadillas-Delgado[5,6], Maria Teresa Fernandez-Diaz[5]

[1] Dipartimento di Scienze della Terra, Università degli Studi di Milano,
Via Botticelli 23, I-20133 Milano, Italy
[2] CNR-Istituto di Cristallografia, Via Amendola 22/O, I-70126 Bari, Italy
[3,4] Department of Geosciences Swedish Museum of Natural History, P.O. Box 50 007, SE-104 05
Stockholm, Sweden
[4] Department of Earth Sciences, Sapienza University di Rome, Piazzale A. Moro 5, I-00185, Roma, Italy
[5] Institut Laue-Langevin, 71 Avenue des Martyrs, F-38000 Grenoble, France
[6] Centro Universitario de la Defensa de Zaragoza, ctra Huesca s/n, 50090 Zaragoza, Spain

Corresponding author: diego.gatta@unimi.it

Abstract

Ettringite, ideally $Ca_6Al_2(SO_4)_3(OH)_{12} \cdot 26H_2O$, is recognized as a secondary-alteration mineral and as an important crystalline constituent of the Portland cements, playing different roles at different time scales. It contains more than 40 wt% of H_2O. The crystal structure and crystal chemistry of ettringite were investigated by electron microprobe analysis in wavelength-dispersive mode, infrared spectroscopy and single-crystal neutron diffraction at 20 K. The anisotropic neutron structure refinement allowed the location of (22+2) independent H sites, the description of their anisotropic vibrational regime and the complex H-bonding schemes. Analysis of the difference-Fourier maps of the nuclear density showed a disordered distribution of the inter-column ("free") H_2O molecules of the ettringite structure, modelled (in the structure refinement) with two independent and mutually exclusive configurations. As the disorder is still preserved down to 20 K, we are inclined to consider that as a "static disorder". The structure of ettringite is largely held together by hydrogen bonding: the building units [*i.e.*, SO_4 tetrahedra, $Al(OH)_6$ octahedra and $Ca(OH)_4(H_2O)_4$ polyhedra] are interconnected

35 through extensive network of hydrogen bonds. The ettringite of this study has an almost

36 ideal composition, with 27 H_2O molecules per formula unit and

37 (Mn+Fe+Si+Ti+Na+Ba) < 0.04 atoms per formula unit. The effect of the low-

38 temperature stability of ettringite and thaumasite on the pronounced "Sulphate Attack"

39 of Portland cements, observed in cold regions, is discussed.

40

41 **Key-words**: ettringite, Portland cements, crystal chemistry, single-crystal neutron

42 diffraction, infrared spectroscopy, hydrogen bonding.

43

44   **Introduction**

45   Ettringite, with ideal chemical formula reported in the literature

46 $Ca_6Al_2(SO_4)_3(OH)_{12} \cdot 26H_2O$ [$a \sim 11.2$ Å, $c \sim 21.3$ Å, space group $P31c$ or $P6_3/mcm$, $Z =$

47 2], occurs in metamorphosed limestone (near igneous contacts or in xenoliths) or as a

48 low-temperature secondary-alteration phase (*e.g.*, weathering crusts on larnite rocks),

49 usually associated with portlandite, afwillite, hydrocalumite afwillite, hydrocalumite,

50 mayenite, and gypsum. It is expected to form a solid solution with thaumasite,

51 $Ca_3Si(OH)_6(CO_3)(SO_4) \cdot 12H_2O$ (Moore and Taylor 1970; Barnett et al. 2000).

52   More than in Nature, an ettringite-like phase is an important crystalline

53 constituent of the Portland cements, and it plays different roles at different time scales.

54 In early hydration stages, the crystallization of ettringite governs the set rate of the

55 calcium aluminate phase ("C3A", $Ca_3Al_2O_6$), which is highly reactive (Taylor 1997;

56 Renaudin et al. 2007). In aged cements, delayed formation of ettringite and thaumasite

57 can promote destructive processes, especially in cement products in which limestone is

58 used as a filling material (Hartshorn et al. 1999) and a diffusion of sulphate-rich fluids

59 occurs (*e.g.,* by contact with sulphate-rich soils or groundwater) (Crammond 1985). The

60   main cement hydration products, *i.e.*, calcium silicate or aluminate hydrates (the so-

61   called C-S-H and C-A-H) and calcium hydroxide (portlandite $Ca(OH)_2$), are

62   decomposed as a result of both sulphate attack and carbonation: as C-S-H and C-A-H

63   provide most of the binding strength, the formation of ettringite and thaumasite leads to

64   weakening and disintegration of the cement matrix. This phenomenon is more

65   pronounced in cement structures below ground (*e.g.*, Hartshorn et al. 1999; Bensted

66   1999; Hobbs and Taylor 2000; Santhanam et al. 2001; Zhang et al. 2009; Gatta et al.

67   2012). The effect of carbonate ions on delayed ettringite formation was recently

68   reported by Asamoto et al. (2017).

69   The crystalline structure of ettringite has been previously investigated by several

70   authors by single-crystal or powder X-ray diffraction (*e.g.*, Moore and Taylor 1968,

71   1970; Goetz-Neunhoeffer and Neubauer 2006) and by neutron powder diffraction

72   (Hartman and Berliner 2006). Its crystal structure is significantly complex (Fig. 1): it

73   consists of $[Ca_3[Al(OH)_6] \cdot 12H_2O]$-columns, parallel to [001], and connected by

74   sulphate groups *via* hydrogen bonds with H_2O molecules. In each column, $Al(OH)_6$-

75   octahedra alternate with triplets of calcium polyhedra with coordination number CN =

76   8, *i.e.,* coordinated by 4 (OH)-groups and 4 H_2O molecules disposed around the 3-fold

77   axis. Disordered distribution affecting the inter-column H_2O molecules was reported

78   and even the disordered distribution of the building groups would lead to a different

79   symmetry of the structure (Moore and Taylor 1970). The structure of a synthetic

80   ettringite-type compound, $Ca_6[Al(OD)_6]_2(SO_4)_3 \cdot 25.5D_2O$, was re-investigated by

81   Hartman and Berliner (2006) by neutron powder diffraction. The authors were able to

82   locate the proton sites with a structure model in the space group *P*31*c*. However, all the

83   sites were modelled isotropically, with unusually different displacement factors for

84 atoms of the same ionic groups, and some of the refined site occupancy factors showing

85 partial occupancies.

86   The aforementioned studies, along with those conducted on the thermal and

87 compressional behaviour of ettringite (*e.g.*, Skoblinskaya and Krasilnikov 1975;

88 Skoblinskaya et al. 1975; Zhou and Glasser 2001; Deb et al. 2003; Hartman et al. 2006;

89 Speziale et al. 2008; Renaudin et al. 2010; Manzano et al. 2012), suggest that: *a)* the

90 hydrogen bonds play an important role for the structural stability of ettringite, but

91 clarification of this role is obscured by the difficulties in locating the protons and thence

92 of refining the bond distances (*i.e.*, O-H) and angles (*i.e.*, O-H···O), *b)* inter-column

93 H_2O could be disordered, but it is still unclear the nature of the disorder (static or

94 dynamic?) and why the H_2O content is found to vary between 24 and 26 molecules per

95 formula unit (*p.f.u.*) (Manzano et al. 2012). In the framework of a long-term project on

96 the sulphate compounds occurring in cements, we have previously described the

97 mechanisms (at the atomic scale) that stabilize the thaumasite structure at low

98 temperature, giving a clue about the reason of the pronounced sulphate attack of

99 Portland cements observed in cold regions (Gatta et al. 2012). To extend our

100 investigations on the second most important compound, which governs the low-*T*

101 sulphate attack in cements, the aim of the present study is a re-investigation of the

102 crystal structure and crystal chemistry of a natural ettringite at low-*T* by means of

103 single-crystal neutron diffraction, infrared spectroscopy and electron microprobe

104 analysis in wavelength-dispersive mode, to define: *a)* the reliable location of all the

105 proton sites and the real topological configuration of the H_2O and (OH)-groups, for a

106 full description of the atomic relationship *via* the H-bonds; *b)* the anisotropic

107 displacement parameters of the H-sites; *c)* the nature of the disordered distribution of

108 the H_2O molecules into structure, and its potential role on the stability of ettringite.

4

109   **Experimental methods**

110   The sample description used in this study, along with the characterization

111   protocols by electron microprobe analysis in wavelength-dispersive mode, powder

112   infrared spectroscopy and anisotropic structure refinement, based on single-crystal

113   neutron diffraction data collected at 20 K, are reported in a section of the

114   Supplementary Materials (*deposited*).

115   -----------------------------------[*Supplementary Materials - Deposited]* -------------------

116   **Experimental methods:**

117   **1) Sample characterization**

118   Ettringite was separate from a specimen from the N'Chwaning mine, Kuruman,

119   Cape Province, Republic of South Africa. The sample (NRM#19950132) is deposited in

120   the mineral collections at the Swedish Museum of Natural History. Large (up to 1.5 cm

121   in length) prismatic, yellow crystals of ettringite and large (up to 1 cm), euhedral, black

122   crystals of braunite-2Q are set on a matrix of fine- to medium-sized (up to 1 mm), pale-

123   red, granular grains of andradite and fine-grained clinochlore.

124   Electron microprobe analyses were obtained by wavelength dispersive

125   spectroscopy (EPMA–WDS) with a Cameca SX50 instrument at the "Istituto di

126   Geologia Ambientale e Geoingegneria, CNR" of Rome, Italy, using the following

127   analytical conditions: accelerating voltage 15 kV, beam current 15 nA, nominal beam

128   diameter 1 μm. Counting time for one spot analysis was 20 s per peak. Standards

129   (element) are: barite (S and Ba), corundum (Al), wollastonite (Ca and Si), magnetite

130   (Fe), rutile (Ti), rhodonite (Mn), jadeite (Na). The PAP routine was applied (Pouchou

131   and Pichoir 1991) for correction of recorded raw data. Ten spot analyses were

132   performed. The studied grain was found to be homogeneous. Chemical data are given in

133   Table 1 (deposited).

134   Ettringite is unstable under the electron beam, showing loss of water, which

135   results in significantly higher concentrations for the remaining constituents. Therefore,

136   Table 1 reports also "normalized" constituents to provide a total of 100 wt%, when

137   combined with the H_2O content calculated on the basis of the neutron structure

138   refinement. The empirical formula, based on 51 anions per formula unit, is:

139    $(Ca_{6.07}Na_{0.01})_{\Sigma 6.08}(Al_{1.95}Fe^{3+}_{0.01}Si_{0.01})_{\Sigma 1.97}(SO_4)_{2.99}(OH)_{12} \cdot 27H_2O$.

140

141   **2) Infrared Spectroscopy**

142   Due to the unstable character of ettringite, no polished single-crystal absorber

143   could be prepared. Attempts to do so resulted in milky crystal slabs, which indicated

144   loss of water. An unpolarized IR spectrum of powdered ettringite in a pressed KBr

145   pellet was recorded in the 600-8000 cm^{-1} at a spectral resolution of 4 cm^{-1} during 32

146   cycles with a Bruker Vertex 70 microscope spectrometer equipped with a glow-bar

147   source, a KBr beam-splitter, and a mid-band MCT detector. A disc of pure pressed KBr

148   prepared under the same conditions was used as a standard. The recorded spectrum is

149   shown in Figure 2.

150

151   **3) Neutron diffraction experiment and structure refinement**

152   A first set of single-crystal neutron diffraction data were collected from a large

153   euhedral fragment of ettringite (approx. 12 mm^3) at a temperature of 20 K on the four-

154   circle diffractometer D9 at the Institut Laue-Langevin (ILL), Grenoble. The wavelength

155   used was 0.8403(1) Å obtained from a Cu(220) monochromator and 1500 reflections

156   were measured with a small two-dimensional area detector up to $2\theta_{max} = 84.6°$, and

157   reduced to 739 unique reflections (Gatta and Fernández-Díaz 2018). The integration,

158   background and Lorentz factor correction of the scans were done with the program

6

159   RACER (Wilkinson et al. 1988). To complete the structural information, the same

160   crystal was placed on a close-cycle refrigerator on the monochromatic four-circle

161   diffractometer D19 at ILL. The wavelength used was 1.454(1) Å, provided by a flat

162   Cu(220) monochromator at $2\theta_M = 69.91°$ take-off angle. The sample was cooled to 20

163   K at 2 K/min cooling rate. The measurement strategy consisted of 22 ω-scans with steps

164   of 0.07° at different χ and φ positions (Fernández-Díaz and Cañadillas-Delgado 2018);

165   reflections up to $2\theta_{max} = 140.4°$ were collected ($\sin\theta/\lambda = 0.597$, max resolution: 0.84 Å).

166   The Multi-Detector Acquisition Data Software (MAD) from ILL was used for data

167   collection. Unit-cell determination [$a = 11.171(1)$ Å, $c = 21.364(1)$ Å] was done by

168   using the PFIND and DIRAX programs, and processing of the raw data was performed

169   using the RETREAT and RAFD19 programs (McIntyre and Stansfield 1988;

170   Duisenberg 1992). Absorption corrections were applied using the D19ABS program

171   (Matthewman et al. 1982). A total number of 14771 Bragg reflections were collected,

172   out of which 1745 reflections were unique for symmetry ($R_{int} = 0.0534$, Laue class -

173     $31m$). Initial structural refinements with SHELX-97 (Sheldrick 1997) showed that

174   extinction was pronounced, but could be reasonably well accounted for by the Larson-

175   like correction (Larson 1967). Other details of the data collections are listed in the CIF

176   (deposited).

177   After preliminary checks about the consistency of the symmetry of the structure

178   models previously reported and the diffraction pattern of this study, the anisotropic

179   structure refinement was performed in the space group $P31c$ using the SHELX-97

180   software (Sheldrick 1997), starting from the structure model of More and Taylor (1970),

181   without any H sites. The neutron scattering lengths of Ca, Al, S, O and H were used

182   according to Sears (1986). Secondary isotropic extinction effects were corrected

183   according to Larson's formalism (1967), as implemented in the SHELXL-97 package

7

184   (Sheldrick 1997). Intense negative residual peaks were found in the difference-Fourier

185   synthesis of the nuclear density when convergence was achieved. Further cycles of

186   refinement were then performed assigning H to these residual peaks (as hydrogen has a

187   negative neutron scattering length). Convergence was slowly achieved and the final

188   least-square cycles were conducted with anisotropic displacement parameters for all the

189   H sites. All the principal mean-square atomic displacement parameters were positively

190   defined. At the end of the last cycle of refinement, no peak larger than $-1.2/+2.2$ fm/Å^3

191   was present in the final difference-Fourier map of the nuclear density (maximum and

192   minimum located near the "disordered" inter-column H_2O sites, see next session and

193   Fig. 3) and the variance-covariance matrix showed no significant correlation among the

194   refined parameters. The structure was refined to R_1 = 0.0881 using 381 refined

195   parameters and 1664 unique reflections with $F_o > 4\sigma(F_o)$. Further details pertaining to

196   the structure refinement (statistical parameters, fractional atomic coordinates and

197   displacement parameters) are reported in the CIF. Relevant bond lengths and angles are

198   listed in Table 2 (deposited).

199   --

200   **Discussion and Implications**

201   The EPMA–WDS analysis is consistent with the crystal chemistry of ettringite

202   obtained in the previous studies, which is unusual in minerals: it contains about 47 wt%

203   H_2O, 19 wt% SO_3, 27 wt% CaO and 8 wt% Al_2O_3, giving a density of only ~1.83

204   g/cm^3. Minor content of Mn, Fe, Si and Ti (in total < 0.02 $a.p.f.u.$, potentially replacing

205   Al, Table 1), along with Na and Ba (in total < 0.02 $a.p.f.u.$, potentially replacing Ca,

206   Table 1), are observed. In other words, ettringite from the N'Chwaning mine shows a

207   composition very close to the end-member formula: $Ca_6Al_2(SO_4)_3(OH)_{12}\cdot 27H_2O$.

8

208   The neutron structure refinement based on the data collected at 20 K is consistent

209   with the general structure model previously obtained (Moore and Taylor 1968, 1970;

210   Goetz-Neunhoeffer and Neubauer 2006; Hartman and Berliner 2006). The present data

211   show that all twenty crystallographically unique oxygen sites in the ettringite structure

212   are involved in hydrogen bonding:

213   -   OW5-OW12, OW19 and OW20 are H_2O-molecule oxygen atoms. OW5-

214   OW11 belong to the coordination shell of two Ca sites (*i.e.*, Ca1: OW6, OW8,

215   OW10, OW12; Ca2: OW5, OW7, OW9, OW11; Fig. 1, see also the CIF). All

216   the H_2O molecules are H bonded, with the following energetically favurable

217   configurations: OW5-H3···O18 (*i.e.*, O18 belonging to a SO_4-group), OW5-

218   H7···O15 (*i.e.*, O15 belonging to a SO_4-group), OW6-H1···O15, OW6-

219   H6···O18, OW7-H12···O16 (*i.e.*, O16 belonging to a SO_4-group), OW7-

220   H17···OW19 (or OW20) (*i.e.*, H_2O···H_2O interaction), OW8-H11···O16,

221   OW8-H13···OW19 (or OW20), OW9-H15···O16, OW9-H16···O15, OW10-

222   H2···O18, OW10-H20···O14 (*i.e.*, O14 belonging to a SO_4-group), OW11-

223   H9···OW9 (*i.e.*, OW9 belonging to a Ca-polyhedron, H_2O···H_2O interaction),

224   OW11-H19···O17 (*i.e.*, O17 belonging to a SO_4-group), OW12-H10···O13

225   (*i.e.*, O13 belonging to a SO_4-group), OW12-H18···OW10 (*i.e.*, OW10

226   belonging to a Ca-polyhedron, H_2O···H_2O interaction), OW19-H21···OW19

227   (or OW20), OW19-H23···OW12 (*i.e.*, OW12 belonging to a Ca-polyhedron,

228   H_2O···H_2O interaction), OW20-H22···OW11 (*i.e.*, OW11 belonging to a Ca-

229   polyhedron, H_2O···H_2O interaction), OW20-H24···OW12 (Table 2). All the H

230   bonds show O···O distances ranging between 2.66 and 2.98 Å (Table 2).

231   -   OH1-OH4 are oxygen atoms of hydroxyl groups, and belong to the

232   coordination shell of the two unique Al sites (Fig. 1, see also the CIF). The

9

233   oxygen atoms of the hydroxyl groups act as donors, forming H-bonds with the

234   H_2O oxygen sites (all belonging to the Ca-coordination shells) as acceptors

235   (*i.e.,* OH1-H8···OW5, OH2-H5···OW6, OH3-H14···OW7 and OH4-

236   H4···OW8, Table 2). All the H-bonds show O···O distances ranging between

237   3.1 and 3.2 Å (Table 2).

238   All the building-block units of the ettringite structure [*i.e.*, SO_4 groups, $Al(OH)_6$

239   octahedra and $Ca(OH)_4(H_2O)_4$ polyhedra] are connected *via* H bonds.

240   The geometry of the H_2O molecule is now well defined: the O-H distances

241   corrected for "riding motion" (Busing and Levy 1964) range between 0.96 and 1.07 Å

242   (Table 2). The H-OW-H angles range between 101.7-109.7° (Table 2), and are all still

243   in the range of the observed H-O-H angles in solid-state materials (Chiari and Ferraris

244   1982; Steiner 1998 and references therein; Gatta et al. 2008). For the hydroxyl groups,

245   the O-H distances corrected for "riding motion" range between 0.94-1.02 Å (Table 2).

246   All the hydrogen bonds show O-H···O angles ≥ 160° (Table 2), a configuration which is

247   energetically less costly (*i.e.*, approaching linearity, Steiner 1998), if compared to that

248   of other minerals (*e.g.*, phyllosilicates, with O-H···O angles ranging between 120°-

249   140°; Gatta et al. 2011, 2013). The oxygen and hydrogen atoms of the H_2O molecules

250   and (OH) groups have slightly larger anisotropic displacement parameters if compared

251   to the other sites populated by Ca, Al or Si; the maximum ratio of the *max* and *min* root-

252   mean-square components of the displacement ellipsoid is observed for the protons of the

253   hydroxyl groups (*i.e.*, OH1-OH4). However, the magnitude of the displacement

254   ellipsoids of the non-H_2O atoms is somehow mitigated by the low *T*.

255   The different Fourier-map of the nuclear density shows a disordered distribution

256   of the inter-column "free" H_2O molecules of the ettringite structure, which was

257   modelled (in the structure refinement) with two independent and mutually exclusive

10

258 configurations: H21-OW19-H23 and H22-OW20-H24 (Fig. 3, see also the CIF). In the

259 structure refinement, the best fit was obtained with *s.o.f.* of 0.48(1) and 0.52(1) for each

260 configuration (then fixed to 0.5 for each one in the last cycles of refinement), leading to

261 a total number of 27 H_2O molecules *p.f.u.*. OW19 and OW20 act as "inter-column

262 bridges", between the Ca-polyhedra (Table 2). As the disorder is still preserved down to

263 20 K, we are inclined to consider that as a "static disorder". We cannot exclude that the

264 H-bonding network of the H_2O molecules promotes the disorder, at least partially: for

265 each of the two configurations (*i.e.*, OW19 and OW20), one of the two protons has an

266 almost ideal H-bonding geometry, the other one not (*i.e.*, with OW-H⋯O ranging

267 between 162-170° *vs.* 144-147°, Table 2). The refined isotropic displacement

268 parameters of the inter-column H_2O sites are likely affected by the positional disorder

269 (presumably overestimated; see the CIF). With the disordered configuration here

270 observed, there is no domain of the structure without the presence of inter-column H_2O

271 molecules, and thus we cannot expect a relevant role of the disorder on the stability of

272 the structure under non-ambient conditions. Furthermore, ettringite with less than 27

273 H_2O molecules *p.f.u.*, if it exists, would behave differently at non-ambient conditions.

274 The structure refinement shows that, in the ettringite structure, the SO_4 tetrahedra

275 are slightly distorted, with $\Delta(S-O)_{max} \sim 0.015$ Å (*i.e.*, the difference between the longest

276 and the shortest bond distances), and the $\Delta(O-S-O)_{max} \sim 1.5°$ (*i.e.*, the difference

277 between the highest and the lowest intra-tetrahedral angle). The $Al(OH)_6$ octahedra are

278 more distorted, with $\Delta(Al1-O)_{max}$ and $\Delta(Al2-O)_{max} \sim 0.045$ Å. The $Ca(OH)_4(H_2O)_4$

279 polyhedra are highly distorted, with $\Delta(Ca1-O)_{max} \sim 0.217$ Å and $\Delta(Ca2-O)_{max} \sim 0.283$ Å

280 (Table 2).

281 The recorded infrared spectrum of ettringite (Fig. 2) shows an intense and broad

282 absorption in the range 3150-3750 cm^{-1} with a maximum at 3427 cm^{-1}. This feature is

283   overprinted by a relatively narrow band at 3638 cm^{-1}. In accordance with the detailed

284   experimental and theoretical analysis of the ettringite vibrational spectra by Scholtzova

285   et al. (2015), the broad absorption feature is assigned to O-H stretching in H_2O, while

286   the narrow band at higher wavenumbers is ascribed to O-H stretching modes in (OH)-

287   groups from the $Al(OH)_6$-octahedra. Absorption at 1640 and 1680 cm^{-1} are caused by

288   bending modes in H_2O. In addition, several absorption bands are observed at lower

289   wavenumbers (*i.e.*, 620, 755, 855, 990 and 1114 cm^{-1}). The recorded spectrum is similar

290   to those previously reported (*e.g.*, Frost et al. 2013; Scholtzova et al. 2015). The

291   assignment of the observed bands, based on the work by Scholtzova et al. (2015), is

292   summarized in Table 3. The splitting of the H-O-H bending mode was explained by

293   Scholtzova et al. (2015) by the presence of the "non-equivalent" H_2O molecules in the

294   crystal structure, related to different hydrogen bond strength and different structural

295   environment. Typical absorption bands in the range 1200-1250 cm^{-1} caused by $B(OH)_4$-

296   groups in ettringite group minerals (Chukanov and Chervonnyi 2016) are not observed

297   in the spectrum of the present sample.

298   Diffraction and spectroscopic findings of this study suggest that the structural

299   stability of ettringite is mainly governed by the hydrogen-bonding geometry, as all of

300   the major building units (*i.e.*, SO_4, $Al(OH)_6$, Ca-polyhedra) are held together by

301   hydrogen bonds. Similar findings were reported for thaumasite (Gatta et al. 2012). This

302   can explain the modest stability of ettringite at high temperature (with structure

303   collapsing at *T* < 150 °C; Zhou and Glasser 2001) or at high pressure (evidence of

304   amorphization were observed at *P* ~ 3 GPa; Clark et al. 2008), likely reflecting the

305   incapacity of the H-bonding scheme to be preserved even at modest high-

306   temperature/high-pressure conditions. In contrast, low *T* stabilizes the ettringite

307   structure, as corroborated by the H-bonding configuration, similarly to what already

12

308   observed for thaumasite (Gatta et al. 2012). We can then extend even to ettringite the

309   same considerations reported by Gatta et al. (2012) on thaumasite: pronounced sulphate

310   attack of Portland cements, observed in cold regions, takes place likely in response to

311   favorable nucleation and growth of ettringite and thaumasite under such conditions.

312   However, whereas the sulphate attack of cement promoted by percolation of sulphate-

313   rich fluids can be potentially mitigated, by isolating the cement structures, it is difficult

314   to prevent the delayed formation of ettringite and thaumasite promoted by the chemical

315   components that already occur in cement paste.

316   We expect that the revised structural model, here obtained, will be employed for a

317   more efficient identification and quantification of ettringite in polyphasic mixtures such

318   as Portland cements. In addition, as the ettringite crystal morphology was observed to

319   affect the expansion of cement structures (Tosun and Baradan 2010), the structure

320   model here derived would deliver a valuable contribution to investigate any potential

321   correlation between the ettringite's habit and its crystal structure, for example *via*

322   periodic-bond-chain development (*e.g*., Hartman and Chan 1993).

323

329

330

331

332

333 **References**

334 Asamoto, S., Murano, K., Kurashige, I., and Nanayakkara, A. (2017) Effect of

335   carbonate ions on delayed ettringite formation. Construction and Building

336   Materials, 147, 221–226.

337 Barnett, S.J., Adam, C.D., and Jackson, A.R.W. (2000) Solid solutions between

338   ettringite, $Ca_6Al_2(SO_4)_3(OH)_{12}\cdot26H_2O$, and thaumasite

339      $Ca_3SiSO_4CO_3(OH)_6\cdot12H_2O$. Journal of Material Science, 35, 4109–4114.

340 Bensted, J. (1999) Thaumasite — background and nature in deterioration of cements,

341   mortars and concretes. Cement and Concrete Composites, 21, 117–121.

342 Busing, W.R. and Levy, H.A. (1964) The effect of thermal motion on the estimation of

343   bond lengths from diffraction measurements. Acta Crystallographica, 17, 142–

344   146.

345 Chiari, G. and Ferraris, G. (1982) The water molecules in crystalline hydrates studied

346   by neutron diffraction. Acta Crystallographica, B38, 2331–2341.

347 Chukanov, N.V. and Chervonnyi, A.D. (2016) Infrared Spectroscopy of Minerals and

348   Related Compounds. Springer International Publishing Switzerland.

349 Clark, S.M., Colas, B., Kunz, M., Speziale, S., and Monteiro, P.J.M. (2008) Effect of

350   pressure on the crystal structure of ettringite. Cement and Concrete Research, 38,

351   19–26.

352 Crammond, N.J. (1985) Thaumasite in failed cement mortars and renders from exposed

353   brickwork. Cement Concrete Research, 15, 1039–1050.

354 Deb, S.K., Manghnani, M.H., Ross, K., Livingston, R.A., and Monteiro, P.J.M. (2003)

355   Raman scattering and X-ray diffraction study of the thermal decomposition of an

356   ettringite-group crystal. Physics and Chemistry of Minerals, 30, 31-38.

357   Duisenberg, A.J.M. (1992) Indexing in single-crystal diffractometry with an obstinate

358   list of reflections. Journal of Applied Crystallography, 25, 92–96.

359   Fernández-Díaz, M.T. and Cañadillas-Delgado, L. (2018) Structure of ettringite;

360   Experimental Report - Institut Laue-Langevin (ILL): Grenoble, 2018; DOI:

361   10.5291/ILL-DATA.TEST-2828.

362   Frost, R.L., López, A., Xi, Y., Scholz, R., Magela da Costa, G., Fernandes Lima, R.M.,

363   and Granja, A. (2013) The spectroscopic characterization of the sulphate mineral

364   ettringite from Kuruman manganese deposits, South Africa. Vibrational

365   Spectroscopy, 68, 266–271.

366   Gatta, G.D. and Fernández-Díaz, M.T. (2018) New insight into the crystal structure of

367   ettringite: $Ca_6[Al(OH)_6]_2(SO4)_3 \cdot 26H_2O$; Experimental Report - Institut Laue-

368   Langevin (ILL): Grenoble, 2018; DOI: 10.5291/ILL-DATA.5-11-419.

369   Gatta, G.D., Rotiroti, N., McIntyre, G.J., Guastoni, A., and Nestola, F. (2008) New

370   insights into the crystal chemistry of epididymite and eudidymite from Malosa,

371   Malawi: a single-crystal neutron diffraction study. American Mineralogist, 93,

372   1158–1165.

373   Gatta, G.D., McIntyre, G.J., Sassi, R., Rotiroti, N., and Pavese, A. (2011) Hydrogen-

374   bond and cation partitioning in $2M_1$-muscovite: A single-crystal neutron-

375   diffraction study at 295 and 20 K. American Mineralogist, 96, 34–41.

376   Gatta, G.D., McIntyre, G.J., Swanson, G.J., and Jacobsen, S.D. (2012) Minerals in

377   cement chemistry: a single-crystal neutron diffraction and Raman spectroscopic

378   study of thaumasite, $Ca_3Si(OH)_6(CO_3)(SO_4) \cdot 12H_2O$. Am. Mineral., 97, 1060–

379   1069.

380   Gatta, G.D., Merlini, M., Valdrè, G., Liermann, H-P., Nénert, G., Rothkirch, A.,

381   Kahlenberg, V., and Pavese, A. (2013) On the crystal structure and compressional

15

382   behaviour of talc: a mineral of interest in petrology and material science. Physics

383   and Chemistry of Minerals, 40, 145–156.

384   Goetz-Neunhoeffer, F. and Neubauer, J. (2006) Refined ettringite

385    $(Ca_6Al_2(SO_4)_3(OH)_{12} \cdot 26H_2O)$ structure for quantitative X-ray diffraction analysis.

386   Powder Diffraction, 21, 4–11.

387   Hartman, M.R., and Berliner, R. (2006) Investigation of the structure of ettringite by

388   time-of-flight neutron powder diffraction techniques. Cement and Concrete

389   Research, 36, 364–370.

390   Hartman, M.R., Brady, S.K., Berliner, R., and Conradi, M.S. (2006) The evolution of

391   structural changes in ettringite during thermal decomposition. Journal of Solid

392   State Chemistry, 179, 1259–1272.

393   Hartman, P., and Chan, H-K. (1993) Application of the Periodic Bond Chain (PBC)

394   Theory and Attachment Energy Consideration to Derive the Crystal Morphology

395   of Hexamethylmelamine. Pharmaceutical Research, 10, 1052–1058.

396   Hartshorn, S.A., Sharp, J.H., and Swamy, R.N. (1999) Thaumasite formation in

397   Portland limestone cement pastes. Cement Concrete Research, 29, 1331–1340.

398   Hobbs, D.W. and Taylor, M.G. (2000) Nature of the thaumasite sulphate attack

399   mechanism in field concrete. Cement and Concrete Research, 30, 529–533.

400   Larson, A.C. (1967) Inclusion of secondary extinction in least-squares calculations.

401   Acta Crystallographica, 23, 664 – 665.

402   Manzano, H., Ayuela, A., Telesca, A., Monteiro, P.J.M. and Dolado, J.S. (2012)

403   Ettringite strengthening at high pressures induced by the densification of the

404   hydrogen bond network. Journal of Physical Chemistry, C116, 16138-16143.

16

405   Matthewman, J.C., Thompson, P., and Brown, P.J. (1982) The Cambridge

406   Crystallography Subroutine Library. Journal of Applied Crystallography, 15, 167–

407   173.

408   McIntyre, G.J., and Stansfield, R.F.D. (1988) A general Lorentz correction for single-

409   crystal diffractometers. Acta Crystallographica, A44, 257-262.

410   Moore, A. and Taylor, H.F.W. (1968) Crystal structure of ettringite. Nature, 218, 1048–

411   1049.

412   Moore, A. and Taylor, H.F.W. (1970) Crystal structure of ettringite. Acta

413   Crystallographica, B26, 386–393.

414   Pouchou, J.L. and Pichoir, F. (1991) Quantitative Analysis of Homogeneous or

415   Stratified Microvolumes Applying the Model "PAP". In: Heinrich, K.F.J. and

416   Newbury, D.E., Eds., Electron Probe Quantification, Plenum Press, New York,

417   31–75.

418   Renaudin, G., Sengi, R., Mentel, D., Nedelec, J.M., Leroux, F., and Taviot-Gueho, C.

419   (2007) A Raman study of the sulfated cement hydrates: ettringite and

420   monosulfoaluminate. Journal of Advanced Concrete Technology, 5, 299–312.

421   Renaudin, G., Filinchuk, Y., Neubauer J., Goetz-Neunhoeffer, F. (2010) A comparative

422   structural study of wet and dried ettringite. Cement and Concrete Research, 40,

423   370–375.

424   Santhanam, M., Cohen, M.D., and Olek, J. (2001) Sulfate attack research – wither now?

425   Cement and Concrete Research, 31, 845–851.

426   Scholtzová, E., Kucková, L., Kožíšek J., and Tunega, D. (2015) Structural and

427   spectroscopic characterization of ettringite mineral - combined DFT and

428   experimental study. Journal of Molecular Structure, 1100, 215–224.

429   Sears, V.F. (1986) Neutron Scattering Lengths and Cross-Sections. In K. Sköld and

430   D.L. Price, Eds., Neutron Scattering, Methods of Experimental Physics, Vol. 23A,

431   p. 521-550. Academic Press, New York.

432   Sheldrick, G.M. (1997) SHELX-97. Programs for crystal structure determination and

433   refinement. University of Göttingen, Germany.

434   Skoblinskaya, N.N. and Krastlnikov, K.G. (1975) Changes in crystal structure of

435   ettringite on dehydration. Part 1. Cements and Concretes Research, 5, 381–394.

436   Skoblinskaya, N.N., Krastlnikov, K.G., Nikitina, L.V., and Varlamov, V.P. (1975)

437   Changes in crystal structure of ettringite on dehydration. Part 2. Cement and

438   Concrete Research, 5, 419–432.

439   Speziale, S., Jiang, F., Mao, Z., Monteiro, P.J.M., Wenk, H-R., Duffy, T.S., and

440   Schilling, F.R. (2008) Single-crystal elastic constants of natural ettringite. Cement

441   and Concrete Research, 38, 885–889.

442   Steiner, T. (1998) Opening and narrowing of the water H-O-H angle by hydrogen-

443   bonding effects: Re-inspection of neutron diffraction data. Acta Crystallographica,

444   B54, 464-470.

445   Taylor, H.F.W. (1997) Cement Chemistry, second ed., Thomas Telford, London, 1997.

446   Tosun, K., and Baradan, B. (2010) Effect of ettringite morphology on DEF-related

447   expansion. Cement and Concrete Composites, 32, 271–280.

448   Wilkinson, C., Khamis, H.W., Stansfield, R.F.D., and McIntyre, G.J. (1988) Integration

449   of single-crystal reflections using area multidetectors. Journal of Applied

450   Crystallography, 21, 471–478.

451   Zhang, F.C., Ma, B.G, Yin, G., Wu, Y.Y., and Zhu, Y.C. (2009) Preparation and

452   performance of sulfate resistance cement-based material. Key Engineering

453   Materials, 400, 195–201.

454   Zhou, Q., and Glasser, F.P. (2001) Thermal Stability and Decomposition Mechanisms

455   of Ettringite at < 120°C. Cement and Concrete Research, 31, 1333–1339.

456

457 Table 1 [deposited]. Chemical data for ettringite
458 NRM#19950132, based on EPMA-WDS data and
459 neutron structure refinement.
460

	Measured	Normalized
Na_2O (wt%)	0.04(2)	0.03
CaO	38.7(5)	26.7
BaO	0.01(1)	0.01
Al_2O_3	11.3(2)	7.81
Mn_2O_3	0.02(2)	0.01
Fe_2O_3	0.06(4)	0.04
SiO_2	0.05(5)	0.04
TiO_2	0.01(1)	0.01
SO_3	27.2(6)	18.8
H_2O*		46.55
Total	77.47	100

Number of cations on the basis of 51 anions

Na (*a.p.f.u.*)	0.010
Ca	6.070
Ba	0.001
Al	1.954
Mn^{3+}	0.002
Fe^{3+}	0.007
Si	0.008
Ti^{4+}	0.001
S^{6+}	2.987
H^+	66.000

Note: Errors for oxides are standard deviations (in brackets) of several spot analyses; *a.p.f.u.* = atoms per formula unit.
*H_2O content according to the neutron structure refinement: 27 H_2O molecules *p.f.u.*

490

491

492

493

494

495

496

497

498

499 Table 2 [deposited]. Relevant bond distances (Å) and angles (°) for ettringite based on
500 the neutron structure refinement (data collected at 20 K).
501
502
503

Al1-OH1 (x3)	1.885(9)	OH1-Al1-OH1	87.2(6)	OH3-Al2-OH3	87.3(6)
Al1-OH2 (x3)	1.928(10)	OH1-Al1-OH2	178.7(7)	OH3- Al2-OH4	95.6(2)
Al2-OH3 (x3)	1.877(9)	OH1-Al1-OH2	94.1(2)	OH3- Al2-OH4	92.2(2)
Al2-OH4 (x3)	1.923(10)	OH1-Al1-OH2	93.3(2)	OH3-Al2-OH4	177.0(4)
Ca1-OH3	2.416(5)	OH2-Al1-OH2	85.5(6)	OH4-Al2-OH4	85.0(6)
Ca1-OH1	2.418(6)				
Ca1-OW6	2.443(7)				
Ca1-OW8	2.443(7)	O13-S1-O15	110.2(3)	O17-S3-O18	108.9(3)
Ca1-OH1	2.459(5)	O15-S1-O15	108.8(3)	O18-S3-O18	110.0(4)
Ca1-OH3	2.462(6)				
Ca1-OW10	2.603(5)	O14-S2-O16	109.2(4)		
Ca1-OW12	2.633(5)	O16-S2-O16	109.7(4)		
Ca2-OH4	2.379(5)				
Ca2-OH2	2.407(5)				
Ca2-OH2	2.408(5)				
Ca2-OH4	2.409(5)				
Ca2-OW5	2.432(6)				
Ca2-OW7	2.440(6)				
Ca2-OW9	2.614(4)				
Ca2-OW11	2.662(4)				
S1-O15 (x3)	1.481(4)				
S1-O13	1.491(7)				
S2-O14	1.481(8)				
S2-O16 (x3)	1.486(4)				
S3-O18 (x3)	1.474(4)				
S3-O17	1.490(8)				

OH1-H8	0.973(9)	OW5-H3	0.991(6)	OW5-H7	0.988(8)		
OH1-H8*	1.000(12)	OW5-H3*	1.007(9)	OW5-H7*	1.001(11)		
H8···OW5	2.170(10)	H3···O18	1.780(6)	H7···O15	1.841(9)		
OH1···OW5	3.098(5)	OW5···O18	2.749(4)	OW5···O15	2.822(6)		
OH1-H8···OW5	159.2(7)	OW5-H3···O18	164.8(6)	OW5-H7···O15	171.4(6)		
OH2-H5	0.903(9)	OW6-H1	0.926(6)	OW6-H6	0.937(9)		
OH2-H5*	0.920(11)	OW6-H1*	0.943(9)	OW6-H6*	0.962(12)		
H5···OW6	2.223(9)	H1···O15	1.845(7)	H6···O18	1.890(10)		
OH2···OW6	3.105 (6)	OW6···O15	2.748(4)	OW6···O18	2.805(6)		
OH2-H5···OW6	165.3(7)	OW6-H1···O15	164.3(7)	OW6-H6···O18	164.5(8)		
OH3-H14	0.952(9)	OW7-H12	0.959(9)	OW7-H17	0.954(7)		
OH3-H14*	0.980(12)	OW7-H12*	0.981(12)	OW7-H17*	0.982(10)		
H14···OW7	2.225(10)	H12···O16	1.835(10)	H17···O20	1.734(11)	H17···O19	1.856(11)
OH3···OW7	3.136(6)	OW7···O16	2.779(6)	OW7···O20	2.662(8)	OW7···O19	2.734(7)
OH3-H14···OW7	159.7(7)	OW7-H12···O16	167.5(8)	OW7-H17···O20	163.2(9)	OW7-H17···O19	151.7(8)
OH4-H4	0.936(9)	OW8-H11	0.927(10)	OW8-H13	0.940(9)		
OH4-H4*	0.963(12)	OW8-H11*	0.959(14)	OW8-H13*	0.987(12)		
H4···OW7	2.269(9)	H11···O16	1.824(11)	H13···O19	1.928(12)	H13···O20	2.203(13)
OH4···OW7	3.179(6)	OW8···O16	2.738(6)	OW8···O19	2.822(7)	OW8···O20	3.047(9)
OH4-H4···OW7	163.8(6)	OW8-H11···O16	167.9(9)	OW8-H13···O19	158.2(9)	OW8-H13···O20	149.0(9)
		OW9-H15	0.904(9)	OW9-H16	0.934(8)		
		OW9-H15*	0.930(12)	OW9-H16*	0.951(11)		
		H15···O16	1.804(9)	H16···O15	1.829(8)		
		OW9···O16	2.702(5)	OW9···O15	2.761(5)		
		OW9-H15···O16	172.0(8)	OW9-H16···O15	175.9(7)		
		OW10-H2	0.996(7)	OW10-H20	1.013(9)		
		OW10-H2*	1.016(9)	OW10-H20*	1.039(12)		
		H2···O18	1.816(7)	H20···O14	1.931(8)		
		OW10···O18	2.803(5)	OW10···O14	2.906(5)		
		OW10-H2···O18	170.6(6)	OW10-H20···O14	160.6(7)		
		OW11-H9	0.957(10)	OW11-H19	0.959(8)		
		OW11-H9*	0.967(13)	OW11-H19*	0.975(12)		
		H9···OW9	2.029(11)	H19···O17	1.879(8)		
		OW11···OW9	2.981(7)	OW11···O17	2.821(5)		

21

OW11-H9···OW9	172.9(8)	OW11-H19···O17	166.8(6)
OW12-H10	0.927(9)	OW12-H18	0.926(14)
OW12-H10*	0.957(12)	OW12-H18*	0.968(18)
H10···O13	1.937(10)	H18···OW10	2.068(15)
OW12···O13	2.835(5)	OW12···OW10	2.983(6)
OW12-H10···O13	162.6(8)	OW12-H18···OW10	169.1(11)

OW19-H21	0.982(9)	OW20-H22	0.986(9)	OW19···OW20	0.86(1)
OW19-H23	0.988(8)	OW20-H24	0.981(9)		
H21-OW19-H23	104.4(11)	H22-OW20-H24	103.5(12)		
H21···OW19	1.485(15)	H22···OW11	2.042(11)		
OW19···OW19	2.355(11)	OW20···OW11	2.910(10)		
OW19-H21···OW19	144.5(16)	OW20-H22···OW11	145.7(9)		
H21···OW20	1.747(12)	H24···OW12	1.920(10)		
OW19···OW20	2.630(12)	OW20···OW12	2.869(9)		
OW19-H21···OW20	147.6(16)	OW20-H24···OW12	161.7(9)		
H23···OW12	1.859(9)				
OW19···OW12	2.837(9)				
OW19-H23···OW12	169.9(10)				

* Bond distance corrected for "riding motion" following Busing and Levy (1964)

504
505
506
507
508
509
510
511
512
513
514
515
516
517
518
519
520
521
522
523
524
525
526
527
528
529
530
531
532
533
534

22

Table 3 [deposited]. Assignments of FTIR-bands in ettringite.

Vibrational mode	Wavenumber (cm⁻¹)
ν_{as} (O-H)$_{Al}$ and ν_s(O-H)$_{Al}$	3638
ν_s (O-H)$_w$	3427
δ H-O-H	1680
δ H-O-H	1640
ν_{as} S-O	1114
ν_s S-O and ν_{as} Al-O	990
δ Al-O-H	855
δ Al-(O-H)	755
δ O-S-O	620

535
536
537
538
539
540
541
542
543
544
545
546
547
548
549
550
551
552
553
554
555
556
557
558
559
560
561
562
563
564
565
566
567
568
569
570
571

23

572 Figure 1. (*Top*) The crystal structure of ettringite viewed down [001] based on the
573 neutron structure refinement at 20 K of this study. Displacement-ellipsoid probability
574 factor: 50%. (*Down*) Configuration of the $[Ca_3Al(OH)_6(H_2O)_{12}]$ building-block units
575 forming columns parallel to [001] (*left side*), and of the alternating H_2O and SO_4
576 tetrahedra running along [001] (*right side*).

577

578

579

580

581

582

583

584

585

586

587

588

589

590

591
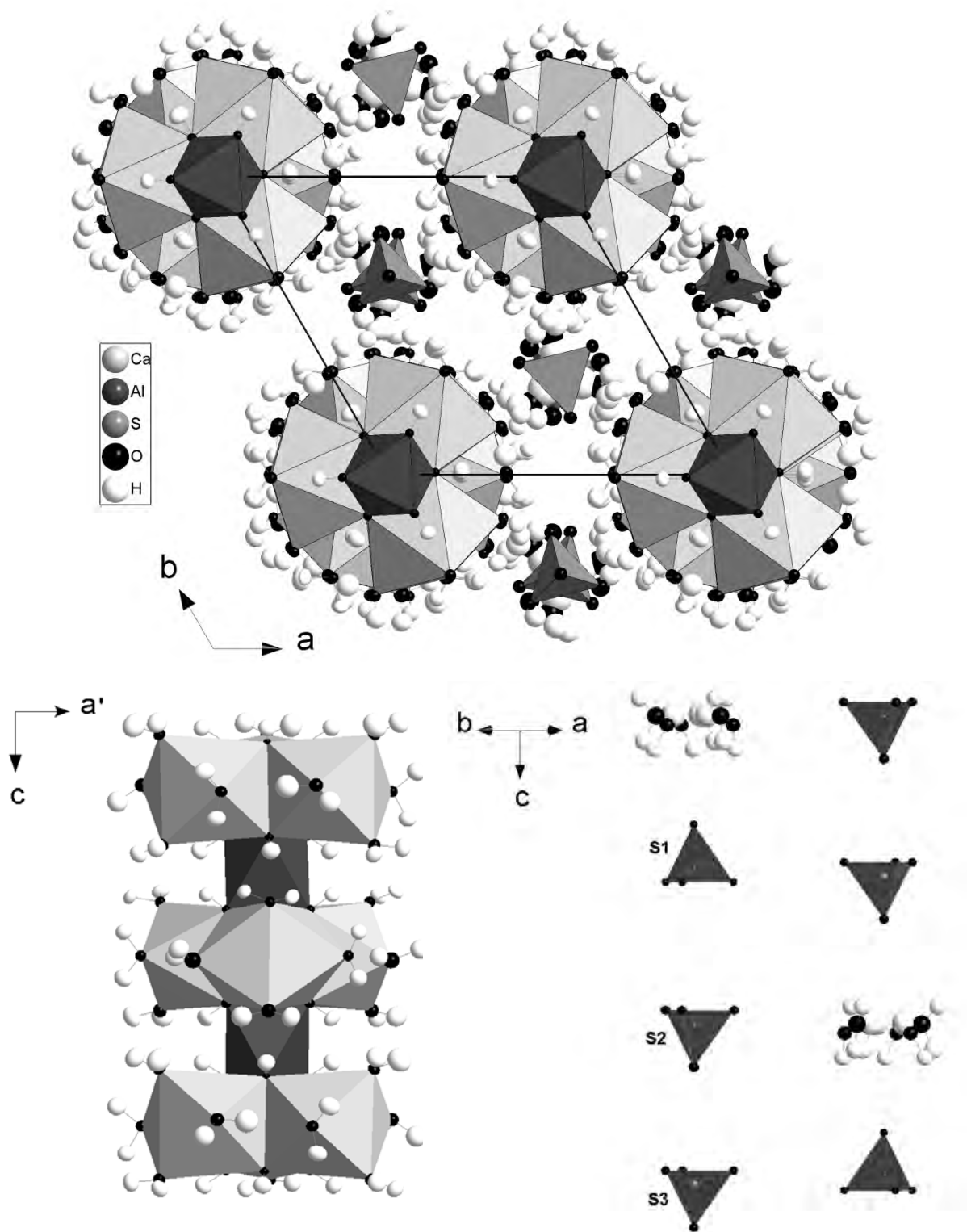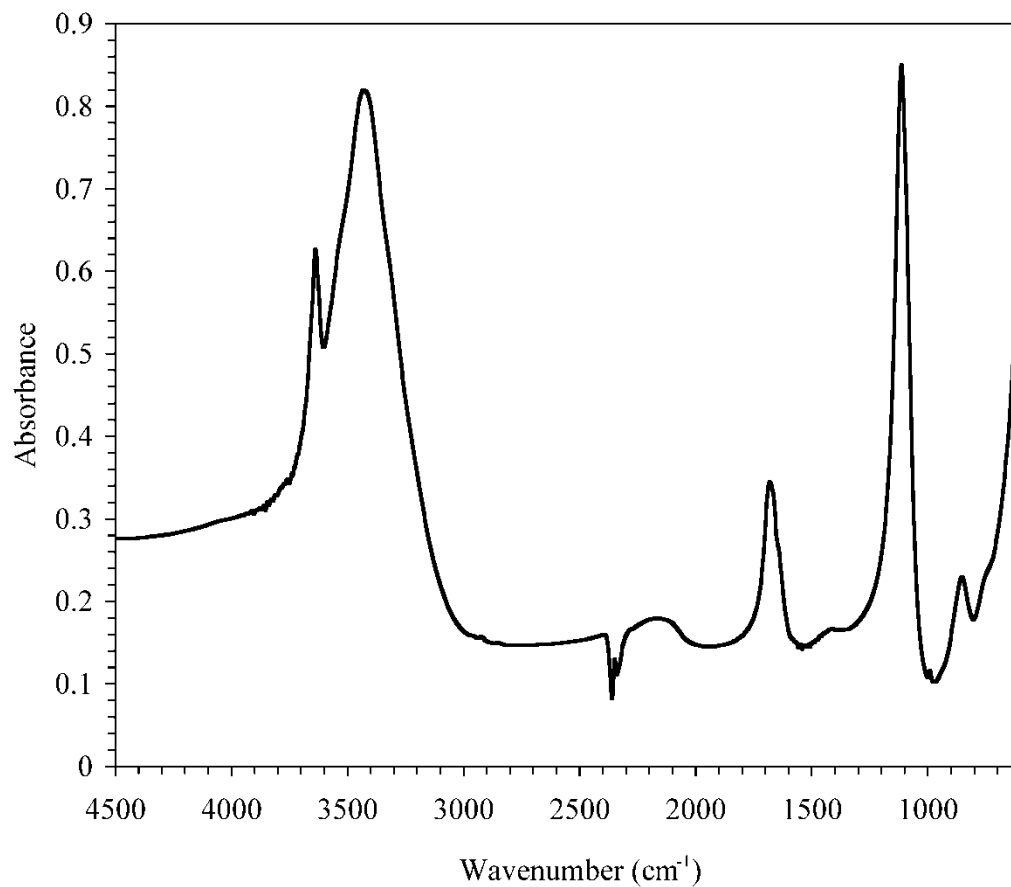
592

593

594

595

596

597

598

599

600

601

602

603

604

605

606

24

607   Figure 2. Infrared spectrum of ettringite.

608
609
610
611
612
613
614
615
616
617
618
619
620
621
622
623
624
625
626
627
628
629
630

631   Figure 3. (*Top*) Difference Fourier maps of ettringite at $z \sim 0.235$ calculated with
632   coefficients Fo-Fc and phased by Fc. The Fc were calculated from a structural model
633   without the inter-column H_2O sites (H21-OW19-H23, H22-OW20-H24; CIF and Table
634   2). Maxima, ascribable to the missing O sites, and minima, ascribable to the missing H
635   sites (as H has negative neutron scattering length), about the 3-fold axis, are visible.
636   Color bar unit: fm/Å^3. (*Down*) Schematic configuration and location of the inter-column
637   H_2O sites.
638
639
640